Applied Energy 342 (2023) 121136

Contents lists available at ScienceDirect

Applied Energy

journal homepage: www.elsevier.com/locate/apenergy

The pinhole effect on proton exchange membrane fuel cell (PEMFC) current density distribution and temperature distribution

Feng Ding [a,b], Tingting Zou [d], Tao Wei [b,c], Lei Chen [b], Xiaoping Qin [b], Zhigang Shao [b,*], Jianjun Yang [d,*]

[a] Department of Chemical Physics, University of Science and Technology of China, Hefei, Anhui 230026, China
[b] Fuel Cell System and Engineering Laboratory, Dalian Institute of Chemical Physics, Chinese Academy of Sciences, Dalian 116023, China
[c] University of Chinese Academy of Sciences, Beijing 100049, China
[d] GPL Photonics Laboratory, State Key Laboratory of Applied Optics, Changchun Institute of Optics, Fine Mechanics and Physics, Chinese Academy of Sciences, Changchun 130033, China

HIGHLIGHTS

- For PEMFCs with pinholes, a local reverse current was found in anode overpressure.
- Local hot spots were found with the same trend as local reverse currents.
- A small pinhole requires more anode overpressure to generate a local reverse current.
- The pinhole exerts an indirect effect on PEMFC performance.

GRAPHICAL ABSTRACT

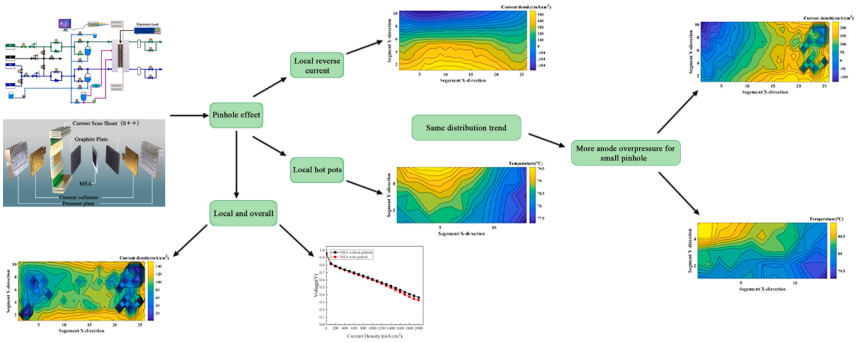

ARTICLE INFO

Keywords:
PEMFC degradation
Pinhole
Local reverse current
Local hot spot
Hydrogen crossover

ABSTRACT

The proton exchange membrane (PEM) is a critical portion of a proton exchange membrane fuel cell (PEMFC). However, it is strongly influenced by pinhole defects owing to degradation during its operation or manufacture. Such defects may accelerate chemical polymer decomposition, eventually causing fuel cell failure and other safety issues. Thus, it is necessary to detect and characterize pinhole degradation while determining the effect of pinhole on electrochemical behavior and fuel cell performance. Herein, pinholes of different sizes (10 and 100 μm) were fabricated on a 50-cm^2 catalyst-coated membrane (CCM) and characterized using commercial current scan shunt (CSS) S++ Simulation Services (Hephas Energy) to investigate the effects of pinhole size on current density and temperature distributions of the PEMFC. Our analyses show that hydrogen crossover from the anode to the cathode through a pinhole can cause hydrogen diffusion and a hydrogen oxidation reaction (HOR) on the cathode electrode surface under certain conditions. Consequently, local reverse currents and hot spots are detected around the pinhole position under open-circuit voltage (OCV) and the corresponding current and temperature distribution trends are uniform. Conversely, the reverse current immediately disappeared from the current distribution map because water exists under operation conditions, resulting in membrane swelling and

* Corresponding authors.
E-mail addresses: zhgshao@dicp.ac.cn (Z. Shao), jjyang@ciomp.ac.cn (J. Yang).

https://doi.org/10.1016/j.apenergy.2023.121136
Received 15 February 2023; Received in revised form 1 April 2023; Accepted 9 April 2023
Available online 2 May 2023

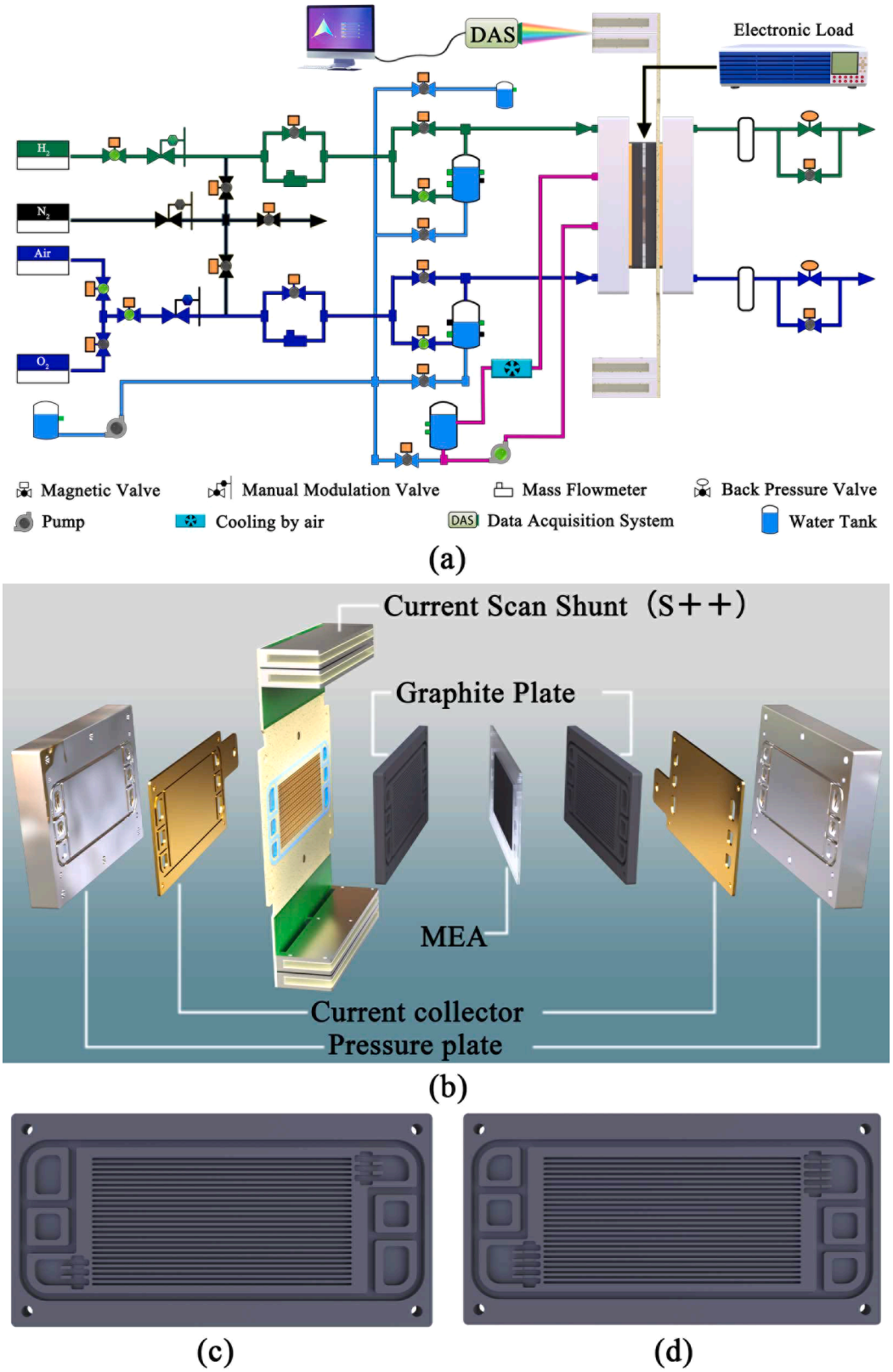

Fig. 1. (a) Schematic showing the single cell test bench. (b) Single cell PCB assembly used for current density and temperature distribution measurements. (c) Anode flow field. (d) Cathode flow field.

pinhole sealing. Thus, hydrogen crossover decreased and local reverse currents reappeared as a result of anode overpressure during fuel cell operation. The local reverse current becomes weaker when using the same-sized pinhole under the same anode overpressure because the overall current density increases. Furthermore, owing to the presence of water, the capillary force for the 100-μm pinhole was higher than that for the 10-μm pinhole,

Table 1
PEMFC parameters and operational conditions.

Parameters(cell design)	Value	Operational conditions	Value
Anode catalyst loading (mg Pt/cm^2)	0.2	Anode gas	Hydrogen
Cathode catalyst loading (mg Pt/cm^2)	0.4	Anode relative humidity	60%
Channel width (mm)	1	Anode stoichiometry	1.5
Channel depth (mm)	1	Anode back pressure	0–1.2 bar
Rib width (mm)	1	Cathode gas	Air/N_2
		Cathode relative humidity	60%
		Cathode stoichiometry	3.5
		Cathode back pressure	0–1 bar
		Cell temperature	80℃

indicating that more anode overpressure is required to generate a local reverse current. Thus, the position and size of the pinhole can be effectively detected using *in situ* characterization.

1. Introduction

Proton exchange membrane fuel cells (PEMFCs) provide clean energy for automobiles, trucks, airplanes, ships, etc [1]. However, currently, the life of a PEMFC is relatively short and is among the main factors hindering its commercial development [2]. PEMFC degradation may arise during operation and includes chemical, physical, and thermal degradations [3–6]. The formation of pinholes in proton exchange membranes (PEMs) is considered a critical factor in PEMFC performance and is one of the main reasons for fuel cell failure and other safety issues. Accidental damage resulting from improper manufacturing processes may generate pinholes in PEMs [7]. Pinhole formation can severely limit the service life of a fuel cell; thus, it is necessary to detect and characterize pinholes as a means to evaluate the effects of pinholes on electrochemical behavior and fuel cell performance. For example, it is important to understand how the local characteristics of hydrogen crossover can affect the overall performance of fuel cells.

The characterization of pinholes in fuel cells caused by degradation or damage can be divided into *in situ* and *ex situ* methods according to the type of operation performed [8–17]. Although these methods are helpful for detecting and characterizing pinholes in fuel cells, they do not fully reveal the influence of pinhole formation on the performance of fuel cells. Furthermore, some of the most common characterization methods are not exclusive to pinholes; for example, a drop in open-circuit voltage (OCV) is not necessarily caused only by the pinhole. Consequently, it is difficult to quantify the degradation of PEMFC caused by pinholes. Additionally, although some *in situ* technologies, such as X-ray computed tomography (XCT) [16], can effectively characterize

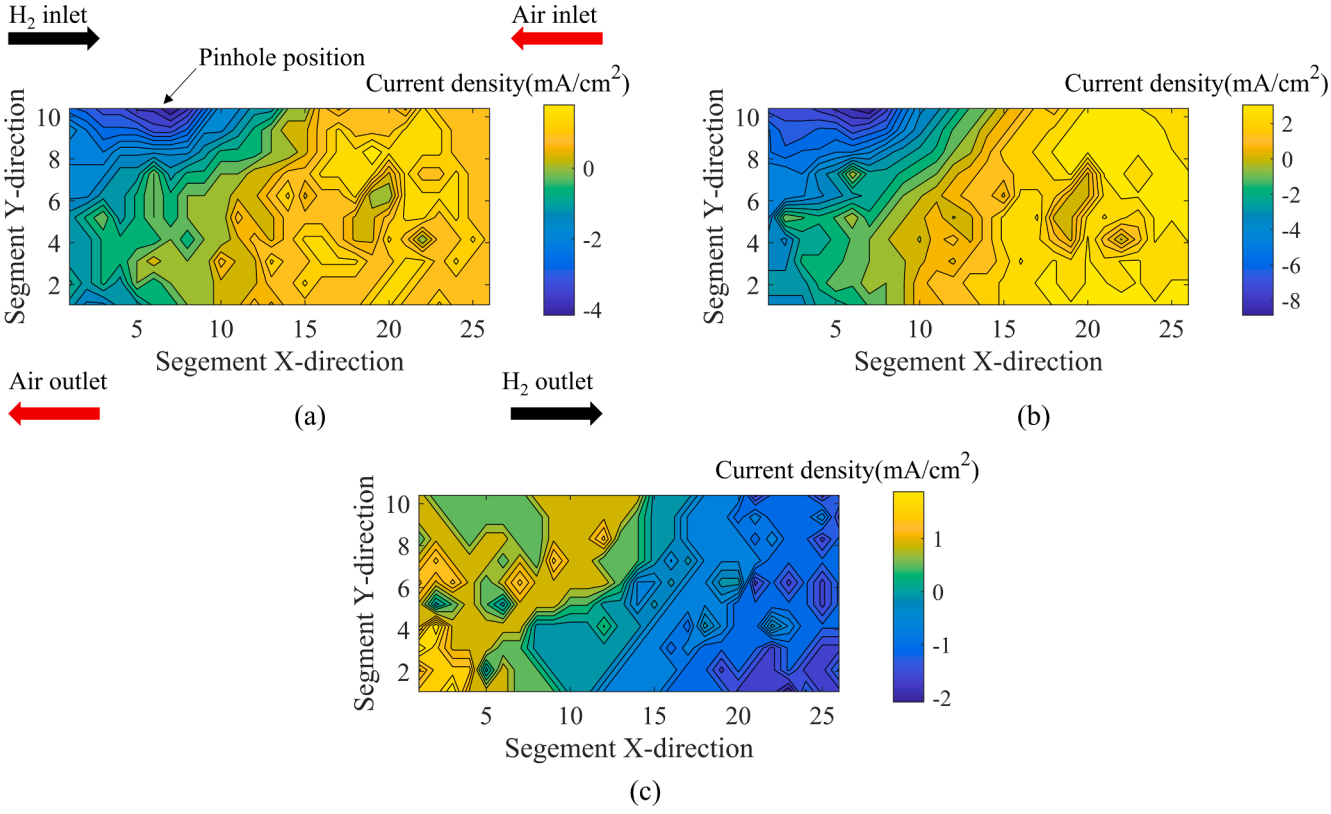

Fig. 2. Current density distribution under OCV conditions. (a) H_2/Air $P_a = P_c = 0$ bar. (b) H_2/Air $P_a = 0.1$ bar, $P_c = 0$ bar. (c) H_2/N_2, $P_a = P_c = 0$ bar.

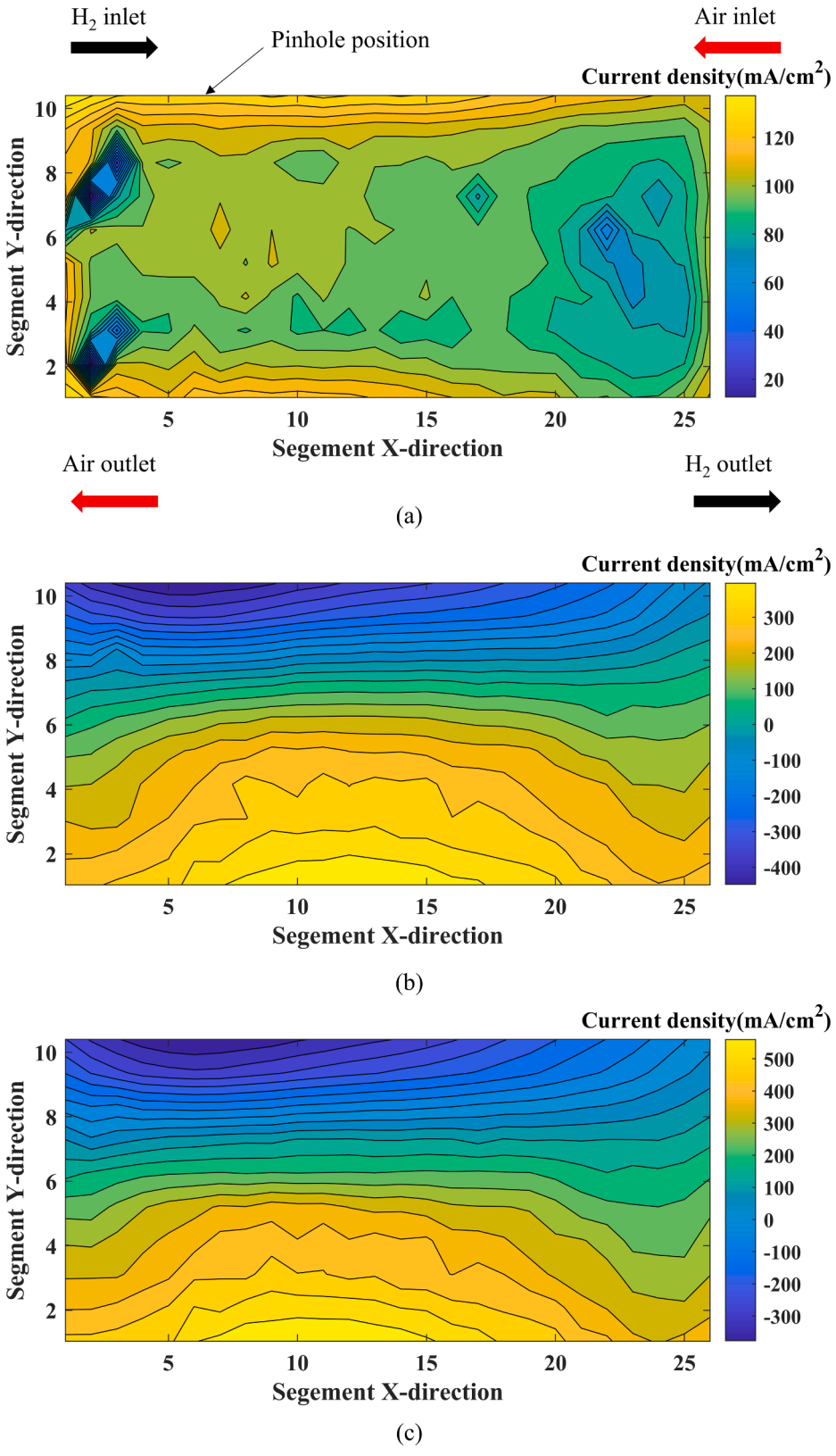

Fig. 3. Current density distribution under operational conditions. (a) 100 mA/cm^2, $P_a = P_c = 1.0$ bar. (b) 100 mA/cm^2, $P_a = 1.4$ bar $P_c = 1.0$ bar. (c) 200 mA/cm^2, $P_a = 1.4$ bar $P_c = 1.0$ bar.

pinholes, they do not reveal the electrochemical behavior caused by pinholes during operation, which in turn influences the performance of fuel cells. Therefore, it is particularly important to *in situ* characterize pinholes in PEMFC, enabling a deeper understanding of their evolution from appearance to the gradual enlargement of pinholes that eventually causes fuel cell failure. IR thermography is a nondestructive technique used for *in situ* characterization that is widely used in detecting fuel cell pinholes [18,19]. However, previous research has shown that pinholes

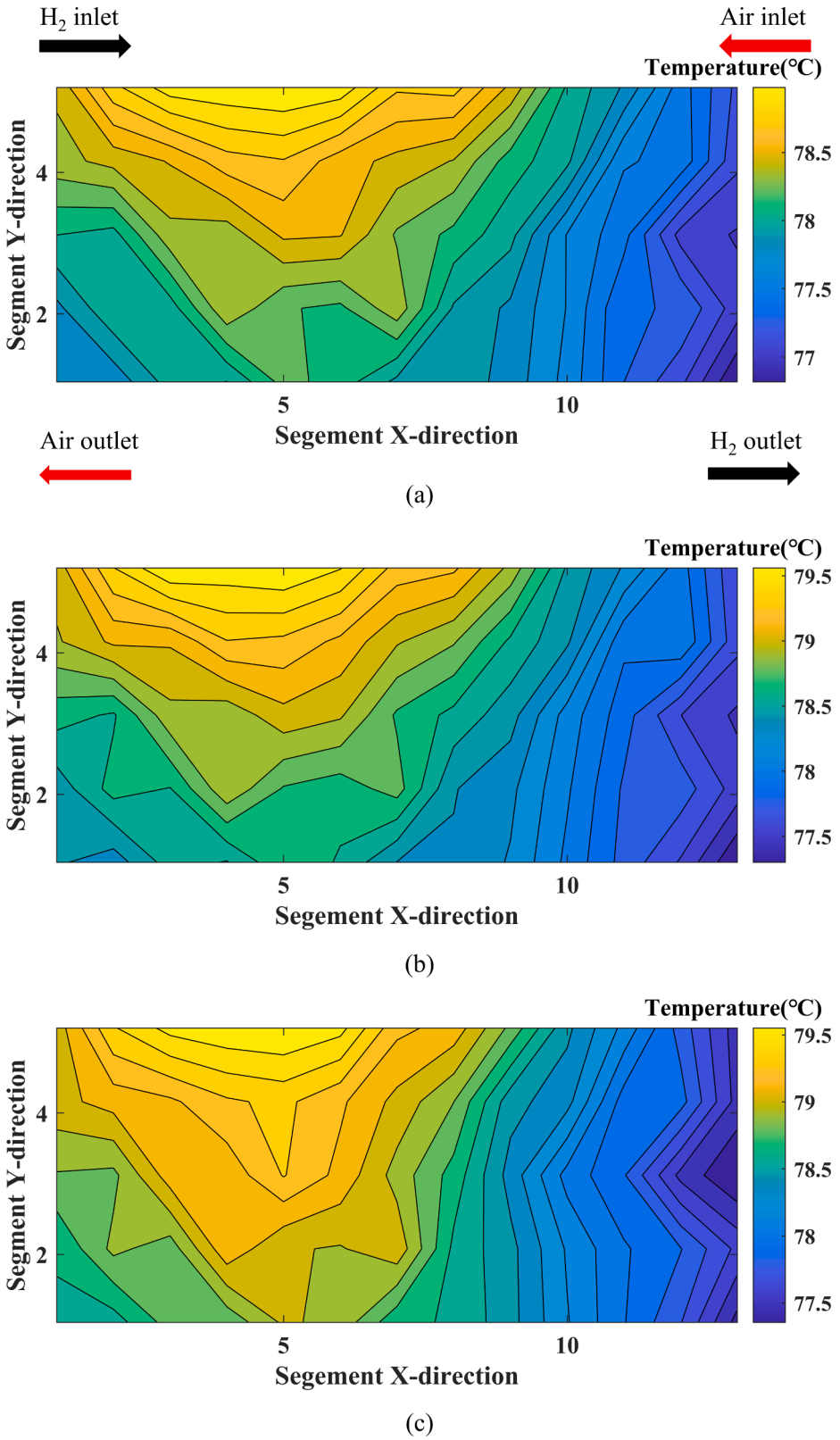

Fig. 4. Temperature distribution under operational conditions. (a) 100 mA/cm^2, $P_a = P_c = 1.0$ bar. (b) 100 mA/cm^2, $P_a = 1.4$ bar $P_c = 1.0$ bar. (c) 200 mA/cm^2, $P_a = 1.4$ bar $P_c = 1.0$ bar.

are not necessarily identified by infrared imaging. The hydrogen crossover phenomenon has been shown to be affected by operating conditions, such as temperature, pressure, and relative humidity [20,21]. In addition to characterization, simulation is an effective way by which the hydrogen crossover phenomenon of fuel cells may be studied [22–28]. Based on theoretical simulations by Weber, Lin et al. [29] used segments of printed circuit board (PCB) technology to characterize fuel cells. However, they only characterized PEMFC at 80 °C under OCV conditions

Table 2
Temperature differences when using a 100-μm pinhole.

Operational condition	Average T (℃)	Minimum T (℃)	Maximum T (℃)	Difference between Max and Ave ΔT (℃)	Difference between Max and Min ΔT (℃)
100 mA/cm^2 (P_a = P_c = 1.0 bar)	78.0732	76.8185	79.0831	1.0099	2.2646
100 mA/cm^2 (P_a – P_c = 0.4 bar)	78.5804	77.3002	79.6730	1.0926	2.3728
200 mA/cm^2 (P_a – P_c = 0.4 bar)	78.6682	77.3548	79.6607	0.9925	2.3059

and at 120 °C during operation under high temperature accelerated stress test conditions; realistic operation temperatures of PEMFC are lower than temperatures used in actual use. Reshetenko et al. [30] studied the current density characteristics of subcells with pinholes under OCV conditions using the segmented cell method; however, segmented cell technology divides the flow field into sections and cannot accurately reveal the distribution of hydrogen gas reaching the cathode surface.

To further study the mechanism of hydrogen crossover, novel characterization methods are required. PCB technology [31–36] can effectively and simultaneously determine current density and temperature distributions, establishing the effect of pinhole on PEMFC current density and temperature distributions.

The existence of pinholes reduces the service life of fuel cells, but traditional detection methods cannot effectively detect and locate such damage. Therefore, this study seeks to use PCB partitioning technology to perform local characterization of PEMFC and *in situ* characterization of pinholes by determining their local electrochemical characteristics. Our approach requires PCB partitions to have more partitions and high resolution. In the experiments reported herein, different sized pinholes were fabricated on a catalyst-coated membrane (CCM) by femtosecond laser technology. Our method enables the effective detection and location of the position and size of pinholes, which has not been previously achieved. This method is not affected by assembly conditions, material properties or flow field, and thus exhibits generality. Additionally, in contrast to most previous studies, which focused on localized hot spots generated by pinholes, we here consider the relationship between localized hot spots generated by pinholes and local reverse currents. Pinholes are shown to have an indirect, rather than direct, effect on the overall performance of PEMFC when the anode and cathode operating pressures are the same; this is contrary to conventional views. Finally, the local reverse current is shown be weakened for the same size pinhole under the same anode overpressure with increasing overall current density, which differs from results previously obtained at high temperature.

Pinholes with different sizes (10 μm and 100 μm) were fabricated on a CCM with an area of 50 cm^2 using a commercial chirped-pulse-amplification fs-laser system (Spitfire Ace, Spectra Physics); pinholes were then characterized using commercial current scan shunt (CSS) S++ Simulation Services (Hephas Energy) to investigate their effect on PEMFC current density and temperature distributions. Our experimental results enable the following aspects to be discussed: 1. pinhole effect on local current density distribution during OCV and operation; 2. pinhole effect on current density and temperature distributions under different back pressure differential conditions for both the anode and cathode; 3. influence of hydrogen crossover on local and global fuel cell performance cells: 4. positional relationship between local current characteristics of the pinhole and local hot spots; and 5. local current and temperature distribution of pinholes with different diameters.

2. Experimental

2.1. Single fuel cell experiment apparatus

The programmable DC electric loader (PLZ664WA, Kikusui) setup used in this experiment is shown in Fig. 1(a). The single cell assembly is shown in Fig. 1(b). A membrane electrode assembly (MEA) was prepared using a CCM and gas diffusion layers (GDLs) *via* the hot pressure method. The PEM was a commercial Gore membrane with a thickness of 18 μm. The MEA active area was 50 cm^2 (5 × 10 cm). The PCB board was placed between the cathode flow field and current collector plate to determine the current density and temperature distributions. The single fuel cell assembly torque was 6.5 N•m. Other specific parameters are given in Table 1.

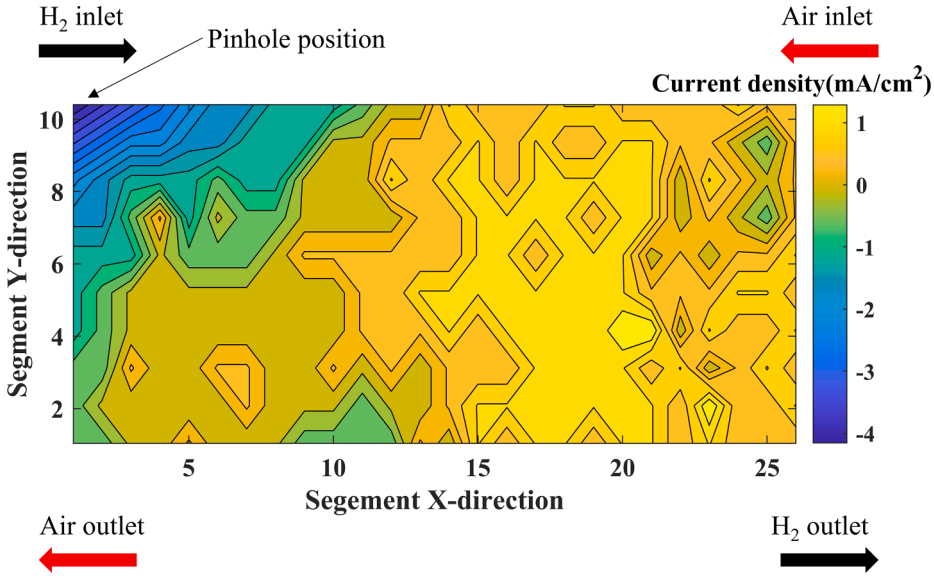

Fig. 5. 10-μm pinhole current density distribution under OCV conditions, i.e., P_a = P_c = 1.0 bar.

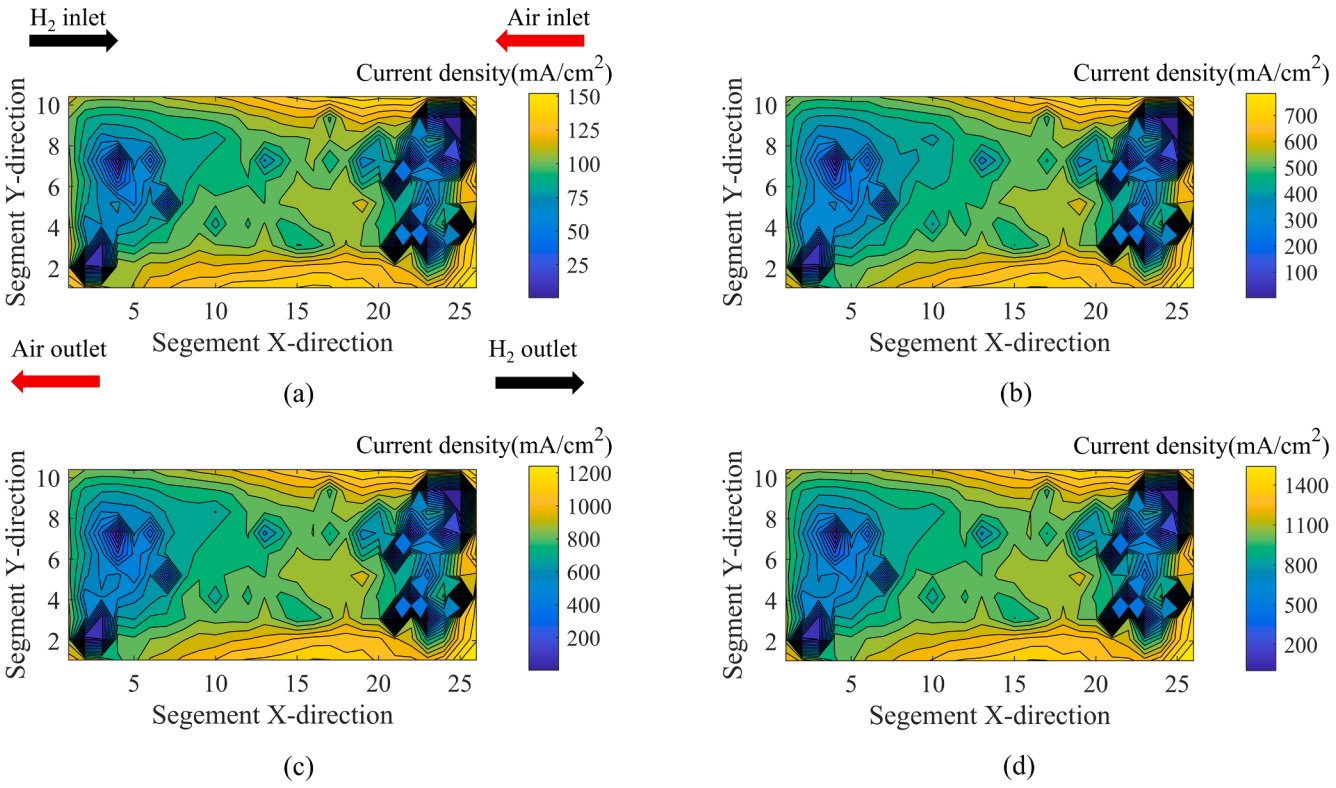

Fig. 6. Current density distribution. (a) 100 mA/cm^2 $P_a = P_c = 1.0$ bar. (b) 500 mA/cm^2 $P_a = P_c = 1.0$ bar. (c) 800 mA/cm^2 $P_a = P_c = 1.0$ bar. (d) 1000 mA/cm^2 $P_a = P_c = 1.0$ bar.

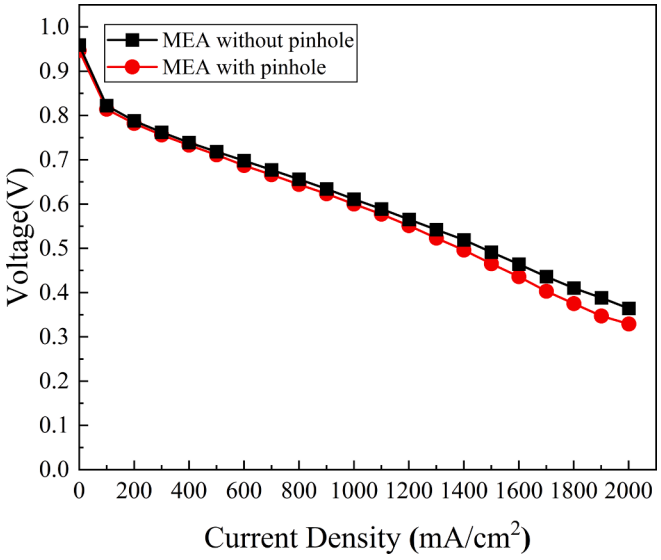

Fig. 7. Polarization curve of MEA without and with 10-μm pinhole.

2.2. Operational conditions

The counter-flow mode was used such that H_2 was fed into the anode and air was fed into the cathode. The anode and cathode flow fields are parallel as shown in Fig. 1(c) for the anode and Fig. 1(d) for the cathode. Other relevant parameters are given in Table 1.

2.3. Current and temperature density distribution

Commercial CSS S++ Simulation Services (Hephas Energy) was used to measure the PEMFC current density and temperature distributions. The PCB has an effective test area of 5 × 10 cm^2, including 26 × 10 current density test points and 13 × 5 temperature test points. Current distribution and temperature distribution data were collected every 500 ms.

The overall assembly is shown in Fig. 1(b). The PCB was placed on one side of the graphite flow field of the fuel cell cathode to ensure good contact with the cathode graphite flow field during assembly. The copper current collector plate had a gilded surface to ensure that its contact resistance is consistent with the flow field.

2.4. Electrochemical characterization

The overall performance of the single cell was characterized using a polarization curve. The polarization curves were tested by measuring the cell voltage when stepping the current density. The operation temperature was set at 80℃ for single cell polarization tests, during which the anode was fed with hydrogen and the cathode was fed with air. The operational back pressure was set at 1.0 bar for both the anode and cathode. Humidity was maintained at 60% for both H_2 and air throughout the experiment. The stoichiometric ratios were 1.5 for H_2 and 3.5 for air.

2.5. Pinhole fabrication

CCM pinholes were fabricated using a commercial chirped-pulse-amplification fs-laser system (Spitfire Ace, Spectra Physics). The corresponding pulses for the 100 and 10 μm pinholes were 200 and 15 mW, respectively. Pinhole position was set at the hydrogen inlet. The MEA was pressed to ensure that the pinhole location was near the hydrogen inlet. The position of the 100 and 10 μm pinholes was slightly different.

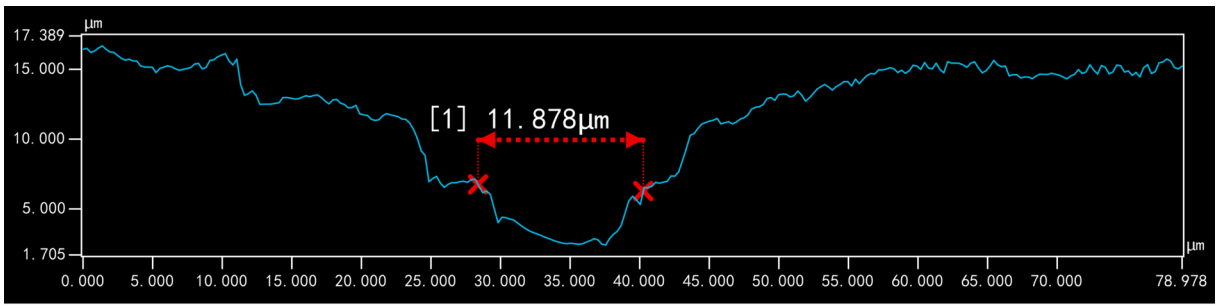

(a)

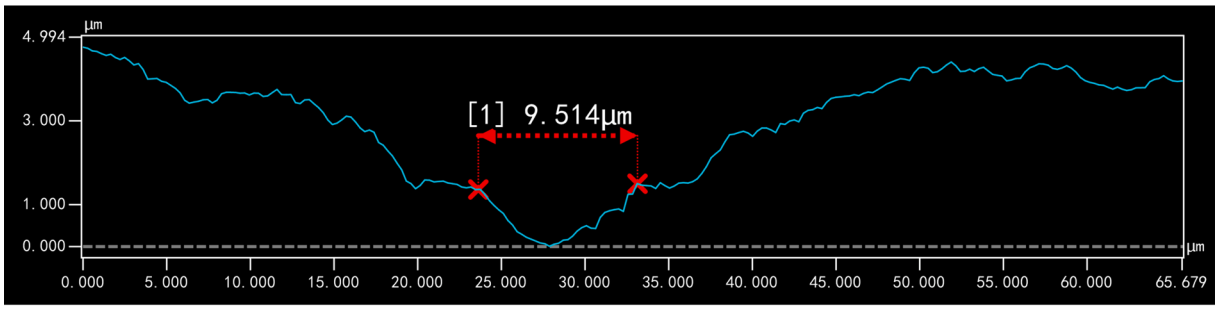

(b)

Fig. 8. (a) Membrane with pinhole under dry conditions. (b) Membrane with pinhole soaked in water at 80 °C for 30 min.

2.6. Pinhole ex situ characterization

The membrane with the 10 μm pinhole was kept under dry conditions, then soaked in 80 ℃ water for 30 min. Both situations were measured using a Keyence VK-X1000.

3. Results and discussion

3.1. Pinhole effect on current density distribution under OCV conditions

First, the effect of pinhole on the current density distribution under OCV conditions was investigated. A femtosecond laser was used to fabricate a pinhole with a diameter of ~100 μm on the CCM to ensure penetration through the entirety of the CCM, and the position was set at the hydrogen inlet. The current density distribution of pinholes under different operational back pressures was obtained by means of anode overpressure. Fig. 2(a) shows the OCV current density distribution under the same operational back pressure for both the anode and cathode ($P_a = P_c = 0$ bar). Fig. 2(b) shows the OCV current density distribution when the anode overpressure and cathode back pressure remained unchanged ($P_a = 0.1$ bar, $P_c = 0$ bar). Fig. 2(a) and 2(b) indicate that a local reverse current appears at the pinhole position and that the local reverse current becomes more obvious as the anode back pressure increases. This result is consistent with the findings of Lin [29] and Reshetenko [30].

Then, nitrogen was introduced to the cathode and the current density distribution was re-measured, as shown in Fig. 2(c). In this test, both the anode back pressure and cathode back pressure were set at 0 bar. The positive and negative values of current density distribution are reversed compared with the H_2–air condition because the hydrogen side has a higher potential than nitrogen and behaves as a concentration cell. According to the Nernst equation, under the condition of H_2–N_2, the potential of the fuel cell is as follows:

$$E_{rest} = -\frac{RT}{2F} ln \frac{P_{H_2}^{cathode}}{P_{H_2}^{anode}}, \quad (1)$$

where E_{rest} is the potential of the fuel cell under the condition of H_2–N_2, R is the ideal gas constant, T is the cell temperature, F is the Faraday constant, $P_{H_2}^{cathode}$ is the partial pressure of hydrogen in the cathode, and $P_{H_2}^{anode}$ is the partial pressure of hydrogen in the anode. Based on this equation, Niroumand et al. [7] effectively adjusted the partial pressure of the anode and cathode to obtain the detectable potential E and then calculated the size of the pinhole using the obtained potential E_{rest}.

3.2. Pinhole effect on current density distribution under operational conditions

A femtosecond laser was used to process a pinhole of ~100 μm on the CCM to ensure the penetration of the whole CCM, and this position was set at the hydrogen inlet. The purpose of this process was to examine the effects of large-sized pinholes on current density distribution under operational conditions.

First, we considered the condition under which the back pressures of the cathode and anode are the same. The current density distribution at a current density of 100 mA/cm^2 is shown in Fig. 3(a), where the back pressures of both the cathode and anode are 1.0 bar. The appearance of pinholes does not cause obvious regularity in the overall current density distribution. The current density distribution is different from the OCV condition. MATLAB calculations show that the maximum local current density is 143.52 mA/cm^2, whereas the minimum local current density is 12.48 mA/cm^2. The position of the pinhole at the hydrogen inlet causes large local hydrogen permeation, yielding a relatively low current density at the hydrogen outlet. Subsequently, the anode back pressure was gradually adjusted to 1.4 bar while the cathode back pressure was kept at 1.0 bar. The current density distribution is shown in Fig. 3(b), indicating that as the back pressure difference between the cathode and anode increases, a negative current appears on the cathode surface. The lowest negative current is − 448.76 mA/cm^2; this current gradually increases along the surface of the cathode, finally reaching a current density of 0 mA/cm^2. Then, the current density increases gradually to a local maximum of 437.84 mA/cm^2. Running under this operating condition for 1 h, the overall current density distribution did not change considerably. Subsequently, the operating conditions remained unchanged, the back pressure difference between the anode and cathode was maintained at 0.4 bar, and the current density was

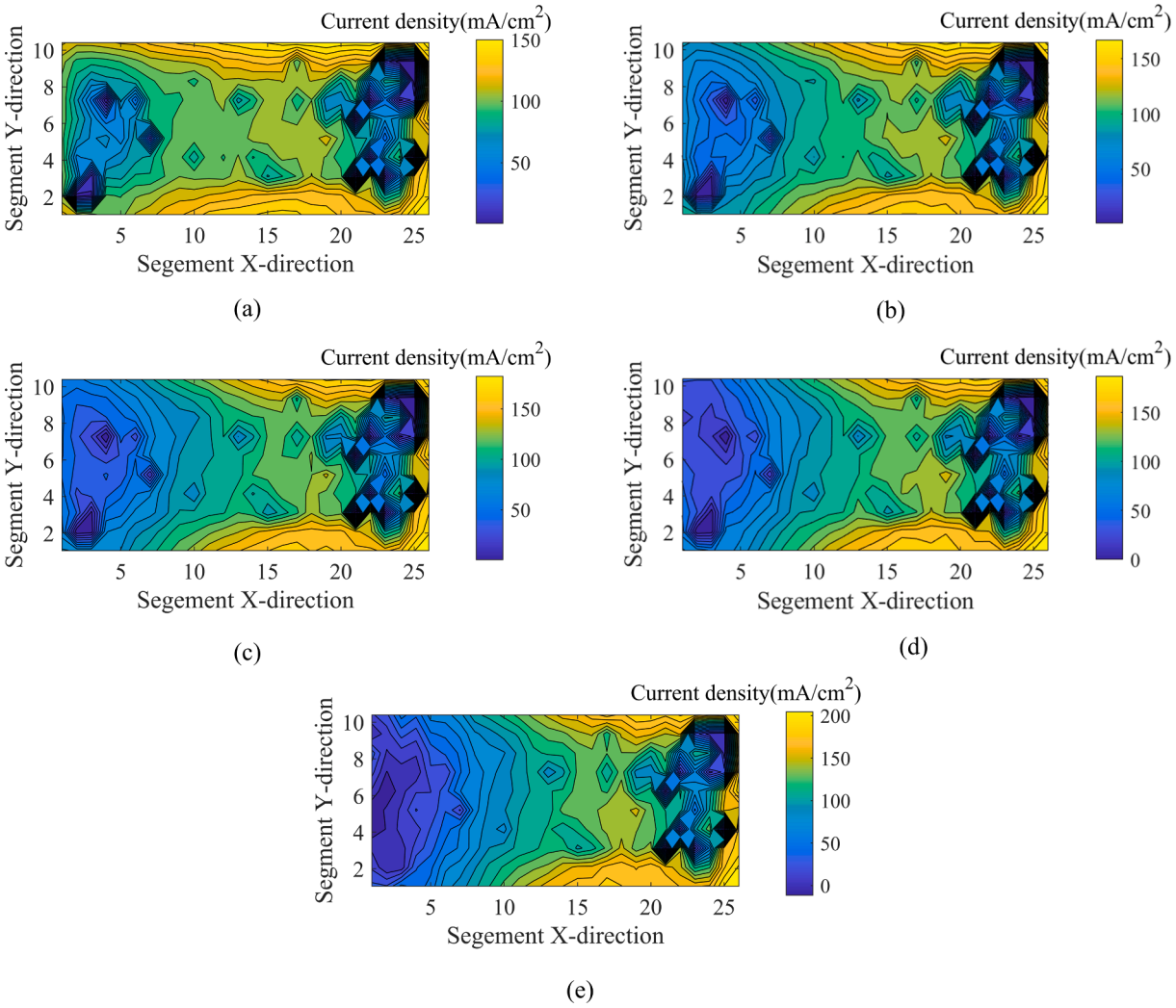

Fig. 9. Current density distribution under 100 mA/cm^2. (a) $P_a - P_c = 0.2$ bar, (b) $P_a - P_c = 0.4$ bar, (c) $P_a - P_c = 0.6$ bar, (d) $P_a - P_c = 0.8$ bar, (e) $P_a - P_c = 1.0$ bar.

increased to 200 mA/cm^2. Fig. 3(c) shows that the overall current density distribution has the same trend as that shown in Fig. 3(b), such that the local current density at the pinhole position is the lowest negative current, −378.04 mA/cm^2, and the negative current at the cathode surface gradually increases as the current density gradually increases, reaching a local maximum current density of 606.84 mA/cm^2. The above experimental phenomena differ from PEMs operated at a high temperature (i.e., 120℃). With increasing current density, the local reverse current caused by pinholes becomes more obvious at high operational temperatures. Conversely, at low temperature (80℃), no local reverse current is detected when the back pressures of the anode and cathode are equal during the fuel cell operation. However, local reverse currents appear when the pressure difference between the anode and cathode backpressure increases and the local reverse current becomes less obvious with increasing overall current density.

This phenomenon may to be explained in three ways: gas diffusion theory; thermodynamics; and electrode kinetics.

Gas diffusion theory: Based on Weber's theory [23], the threshold value of the hydrogen permeability coefficient may be derived for various materials at 120 °C (Teflon 2×10^{-11} mol/bar cm s, Nafion(dry) 3×10^{-11} mol/bar cm s, Nafion(wet) 9×10^{-11} mol/bar cm s, stagnant liquid water 3×10^{-10} mol/bar cm s, and stagnant air 3×10^{-5} mol/bar cm s). Large differences in the transport of hydrogen in different media have been reported. Therefore, under relatively low operational temperatures, owing to the presence of water, the pinholes become sealed and a certain pressure must be applied to the anode to enable hydrogen gas to directly reach the cathode.

The presence of pinholes induces capillary pressure during fuel cell operation, causing liquid water to instantly fill the pinholes. This water sealing effect influences the detection of pinholes. Simultaneously, water acts as a plasticizer for nafion, causing nafion membranes to swell, and reducing the size of the pinholes relative to dry conditions [37]. Therefore, to ensure that hydrogen gas reaches the cathode directly through the pinhole, a certain pressure should be applied to the anode [38]. In Weber simulation [23], the pinholes in the PEM are assumed to be filled with air, i.e., liquid water is not present. By increasing the number of pinholes of smaller size equivalent to the number of pinholes of larger size, Weber deduced that the minimum negative current appeared in the cathode and found that the position of negative current and the highest temperature were the same, i.e., at the pinhole position. When the back pressures of the cathode and anode are unequal, an increase in the overall current density increases the production of liquid water, causing the swelling of the film. Consequently, greater current densities are associated with weaker local reverse currents. Our experimental results show that as long as the liquid water in the pinhole is discharged and the convective movement of hydrogen is increased, the current density and temperature distributions are consistent with Weber's simulations.

Thermodynamics: The cathode electrode of the fuel cell is equipotential, i.e., its potential is equal everywhere. The leakage of hydrogen

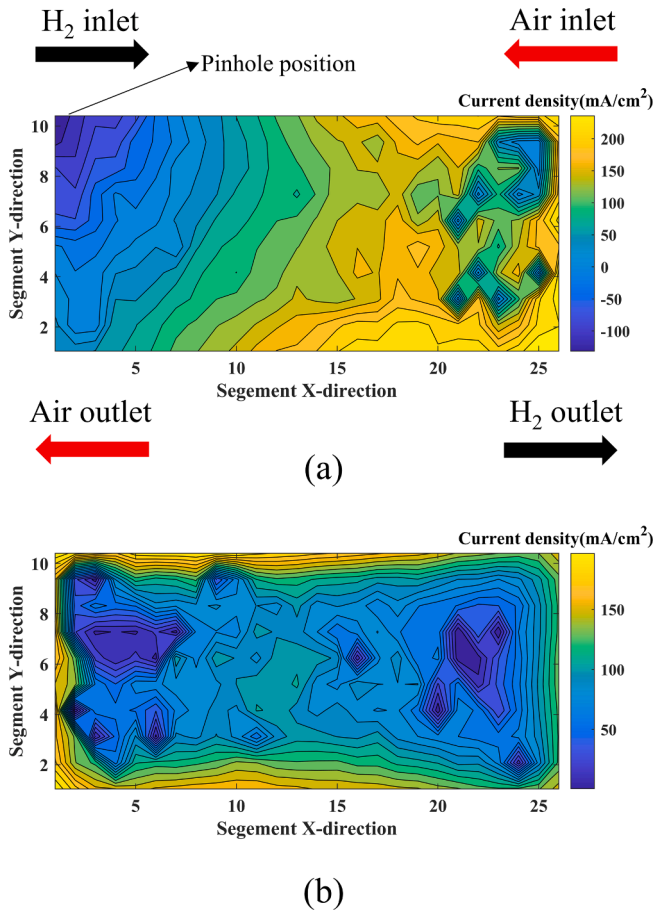

Fig. 10. Current density distribution under 100 mA/cm^2. (a) MEA with and (b) MEA without pinhole at an anode overpressure of 1.2 bar.

from the anode to the cathode generates a mixed potential, such that the change in the mixed potential on the hydrogen side is smaller than that on the oxygen side. The HOR reaction of hydrogen occurs at the surface of the cathode electrode, whereas the oxygen reduction reaction (ORR) reaction of oxygen occurs at the surface of the cathode electrode. The current generated by hydrogen on the cathode is negative relative to that generated by oxygen. About 260 local currents were found to add up to 100 mA/cm^2, i.e., $\sum(i) = i_1 + i_2 + \ldots + i_{260} = 100$ mA/cm^2. Lu et al. [39] investigated changes in OCV under pinhole conditions by changing the pressure difference between the anode and cathode. Their results showed that cathode overpressure causes the OCV to increase slightly, whereas the anode overpressure causes the OCV to decrease. In similar experiments, Kreitmeier et al. [38] investigated cathode and anode overpressures on pinhole conditions, showing that the polarization curve of cathode overpressure did not considerably change, whereas anode overpressure led to a sharp decline in fuel cell performance. The effect of the mixing potential on hydrogen penetration can be explained using the above experiments.

Electrode kinetics: The overpotential and concentration of the reactants determines the reaction rate. The reaction rate of hydrogen oxidation is much faster than that of the overall electrochemical reaction [23]. The HOR reaction rate of hydrogen is 10 mA cm^{-2}, whereas the ORR rate of oxygen is 10^{-8} A cm^{-2}. The reaction rate of hydrogen at the cathode depends on the local concentration of hydrogen and is unaffected by the permeability coefficient of hydrogen.

In summary, regardless of whether thermodynamics or kinetics is considered, hydrogen passage through pinholes is conducive to the HOR reaction at the cathode. Notably, Weber's simulation is based on a pseudo-two-dimensional (2-D) approach. Through our experiment, hydrogen is seen to pass through the pinhole to generate a local reverse current and diffusion behavior is observed at the surface of the cathode electrode. The concentration gradient of hydrogen on the cathode side gradually decreased. As the HOR reaction rate is higher than the ORR reaction rate, ORR plays a dominant role during the consumption of hydrogen and the output of the overall current density must be satisfied such that the local current density below the cell is higher than the output current density.

3.3. Effect of pinhole on temperature distribution

The results of the temperature distribution tests are shown in Fig. 3; data points were collected at the same time as the current density distribution. Fig. 4(a) shows the temperature distribution of 100 mA/cm^2 with a back pressure of 1.0 bar for both the anode and cathode; Fig. 4(b) shows the temperature distribution of 100 mA/cm^2 with a back pressure difference of 0.4 bar between the anode and cathode; Fig. 4(c) shows the temperature distribution of 200 mA/cm^2 with a back pressure difference of 0.4 bar between the anode and cathode. Temperature differences are shown in Table 2.

Hydrogen permeates into the cathode through the pinholes and reacts exothermically with oxygen in the air on the catalyst layer of the cathode. Considering the temperature distribution in Fig. 4 and the data in Table 2, the thermal effects of hydrogen permeation and hydrogen convection are found to be similar, with a difference of approximately 2 °C between the maximum and minimum temperatures. In the present experiment, because a fixed stoichiometric ratio was adopted, the hydrogen gas permeated into the cathode is relatively fixed, such that there is little difference between the maximum and minimum temperatures. The highest temperature appears at the 100 μm pinhole position and the temperature distribution is the same as the overall trend of hydrogen diffusion at the cathode; i.e., the temperature distribution is the same as the trend of the reverse current distribution generated by hydrogen at the cathode. This is consistent with Weber's simulation [40], that is, a temperature gradient distribution exists in the cathode GDLs.

Obermaier et al. [18] investigated temperature differences using IR thermography. Although their approach was able to rapidly locate pinholes in PEMs, the temperature difference caused by the pinhole is subject to various factors, such as electrode properties, GDL properties, and the position of the clamping plate. Haase et al. [41] used the CSS module of the same equipment to test the temperature of the 250 cm^2 short stack; their results showed that the temperature distribution was affected by the coolant. This highlights that there are many factors to be controlled by using temperature differences to detect the pinhole of the fuel cell. Combined with the present experiment, this indicates that IR technology is appropriate for OCV under low humidity and anode overpressure. These conditions ensure increased convection of hydrogen through the pinholes in the fuel cell and the effective detection of the heat release effect.

3.4. Effect of small-sized pinhole on current density distribution under OCV conditions

To further verify the above experimental results, a small pinhole of ~10 μm was fabricated on a CCM using femtosecond laser technology. Under the OCV condition, a local reverse current was generated at the pinhole position (Fig. 5). Similar to Fig. 1(a), a local reverse current was obtained at the pinhole position, with a minimum value of −4.16 mA/cm^2. This indicates that the pinhole position can be located according to the minimum local reverse current. The conditions for small-size pinhole detection were thus determined and may facilitate early diagnosis of PEMFC failure.

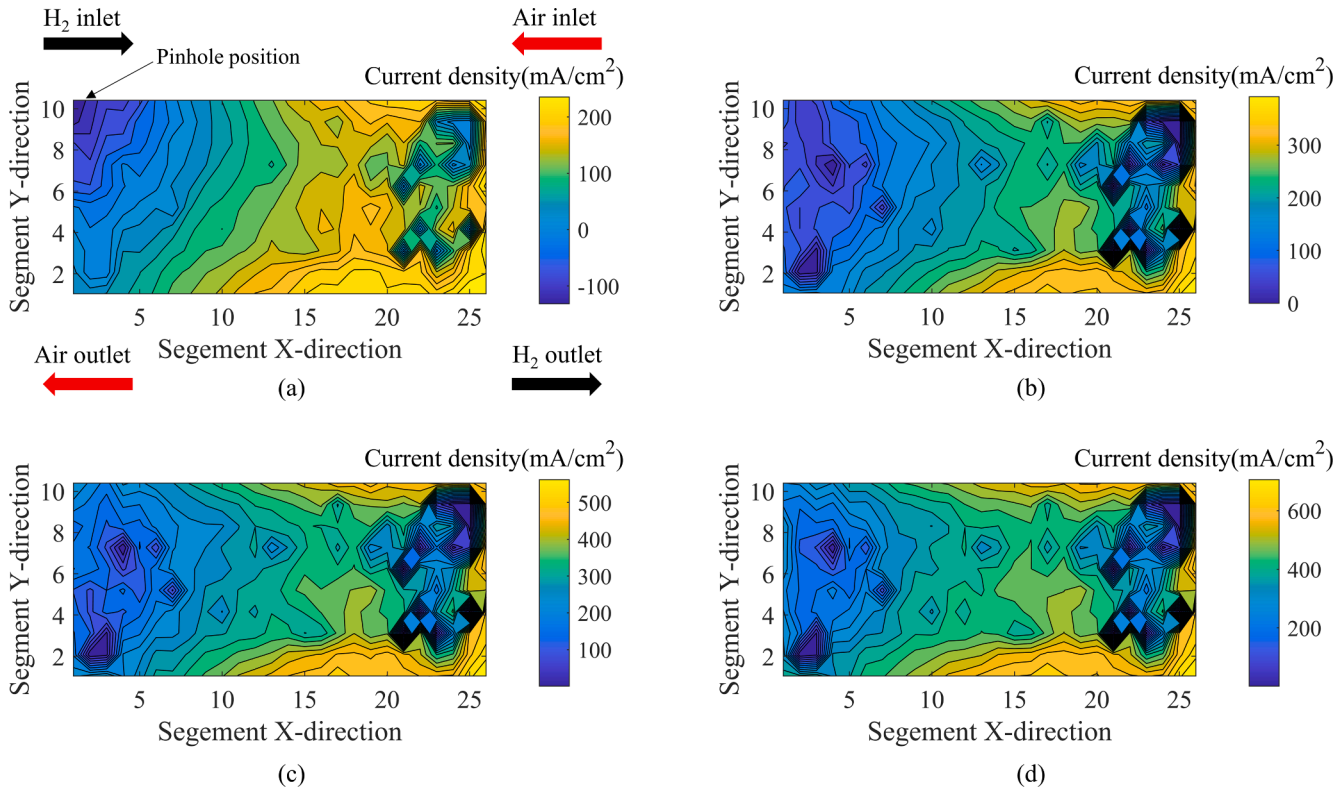

Fig. 11. Current density distributions corresponding to (a) 100 mA/cm^2 $P_a = 1.2$ bar $P_c = 0$ bar, (b) 200 mA/cm^2 $P_a = 1.2$ bar $P_c = 0$ bar, (c) 300 mA/cm^2 $P_a = 1.2$ bar $P_c = 0$ bar, and (d) 400 mA/cm^2 $P_a = 1.2$ bar $P_c = 0$ bar.

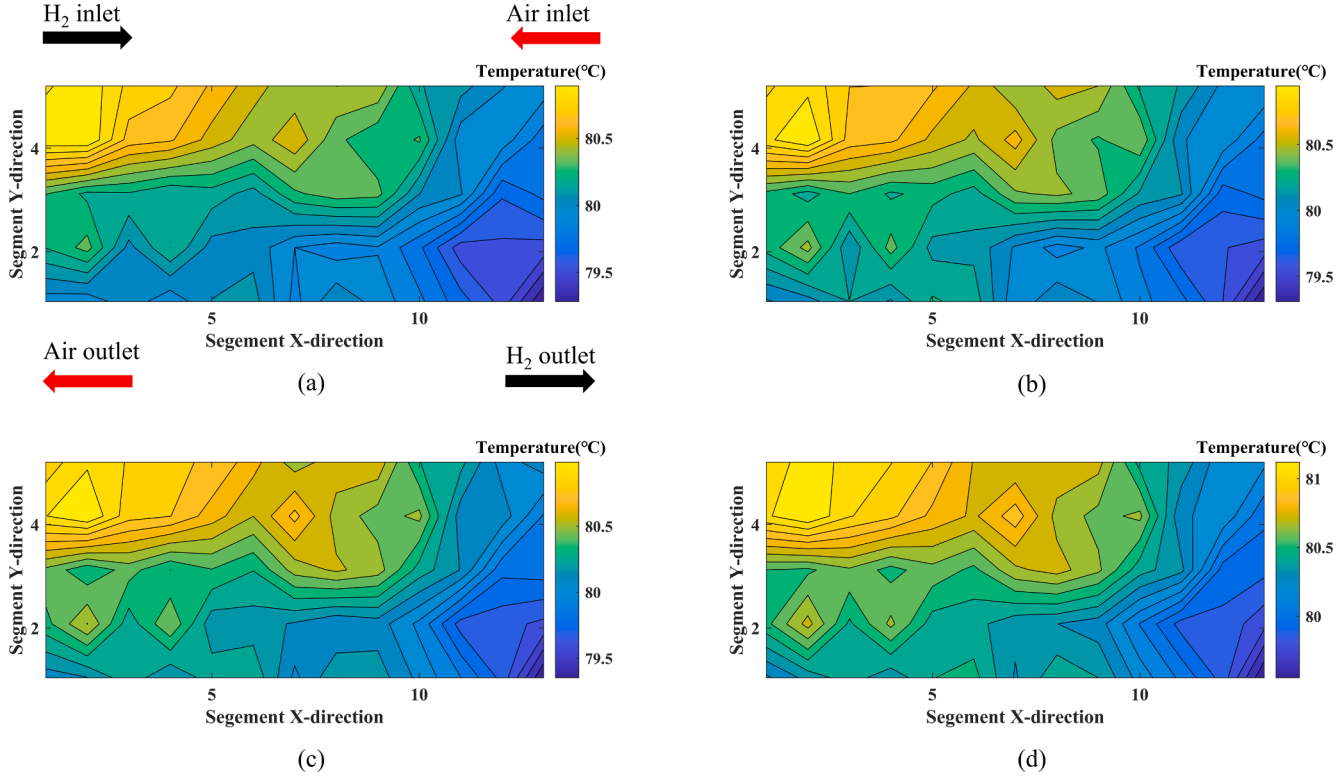

Fig. 12. Temperature distribution corresponding to (a) 100 mA/cm^2 $P_a = 1.2$ bar $P_c = 0$ bar, (b) 200 mA/cm^2 $P_a = 1.2$ bar $P_c = 0$ bar, (c) 300 mA/cm^2 $P_a = 1.2$ bar $P_c = 0$ bar, and (d) 400 mA/cm^2 $P_a = 1.2$ bar $P_c = 0$ bar.

Table 3
Temperature difference when using a 10-μm pinhole.

Operational conditions $P_a - P_c = 1.2$ bar	Average T (℃)	Minimum T (℃)	Maximum T (℃)	Differences between Max and Ave ΔT (℃)	Differences between Max and Min ΔT (℃)
100 mA/cm^2	80.1745	79.2821	80.9706	0.7961	1.6885
200 mA/cm^2	80.2522	79.3099	81.0255	0.7733	1.7156
300 mA/cm^2	80.3352	79.3523	81.0646	0.7294	1.7123
400 mA/cm^2	80.5066	79.5533	81.1965	0.6899	1.6432

3.5. Effects of small-sized pinhole on current density distribution under different current density conditions

The current density distribution owing to small-sized pinholes under different current densities with the same anode and cathode back pressures of 1.0 bar was obtained. As shown in Fig. 6(a)–(d), current density distributions at conditions of 100 mA/cm^2, 500 mA/cm^2, 800 mA/cm^2, and 1000 mA/cm^2, respectively, were obtained. The current density distribution owing to the presence of water and membrane swelling indicates that the reverse current disappears instantaneously when the state is changed from the OCV situation to the 100 mA/cm^2 situation. Meanwhile, the local current performance at the pinhole position itself seems relatively "normal," and the fuel cell can continue operating normally under high current density. Therefore, pinholes are difficult to detect in realistic operational conditions, especially when their size is small. Further, it is inaccurate to judge whether a pinhole exists through the polarization curve [38,39]. Furthermore, the presence of pinholes at the position of the hydrogen inlet leads to a lower local current density at the hydrogen gas outlet and at the air inlet and outlet. When comparing the polarization curve in Fig. 7 with the intact MEA, the OCV of the MEA with pinholes drops slightly at the OCV. Owing to the constant stoichiometric ratios used in the test, a small amount of hydrogen permeates the sealing pinhole to the cathode side, causing fuel starvation at the hydrogen outlet and affording a slight decrease in the overall performance of the cell. Therefore, for PEMFC during operation, owing to the sealing effect of water on pinholes, the impact of pinholes on PEMFC is not direct; it exerts an indirect effect on the performance of the fuel cell.

3.6. Effect of small-size pinholes on current density distribution under different back pressures

The above discussion indicates that the local current density characteristics of the pinhole are obscured owing to the presence of water as well as membrane swelling. Therefore, we can visualize the local current density characteristics of the pinhole by means of anode overpressure according to the following equation:

$$P_c = \frac{2\sigma cos\theta}{r}, \tag{2}$$

where P_c is the capillary pressure, θ is the contact angle of water, r is the pinhole radius, and σ is the surface tension of water. The smaller the radius, the greater the required back pressure difference between the anode and cathode to discharge water from the pinhole. Therefore, the local reverse current can be found by gradually adjusting the back pressure difference between the anode and cathode. Fig. 8 shows an offline test for a 10-μm pinhole under dry and wet conditions, indicating that owing to membrane swelling, the size of the pinhole becomes smaller under wet conditions than under dry conditions.

Fig. 9 shows the cases in which the back pressure differences between the anode and cathode are 0.2, 0.4, 0.6, 0.8, and 1.0 bar. When the pressure difference between the cathode and anode reaches 1.2 bar, a local reverse current occurs. The position of the local reverse current is the same as that of the pinhole, such that the overall current density distribution is similar to the OCV current density distribution. As shown in Fig. 10 (a), when the anode back pressure is 1.2 bar and the cathode back pressure is 0 bar, local reverse current recurrence occurs; this verifies the above hypothesis.

A comparison of Fig. 5 and Fig. 10(a) indicates that when the interference of water is excluded, the current density distribution of OCV shows the same trend as anode overpressure. Local current characteristics can be used to locate pinholes effectively under the condition of anode overpressure during OCV and operation. Both figures accurately show the effect of pinholes on local current. Fig. 10(b) shows the MEA without pinhole at an anode overpressure of 1.2 bar. There is no local reverse current.

3.7. Effect of small-sized pinholes on current density distribution under an anode overpressure 1.2 bar and different current densities

Fig. 11(a)–(d) shows current density distributions under conditions of 100 mA/cm^2, 200 mA/cm^2, 300 mA/cm^2, and 400 mA/cm^2, respectively, with an anode back pressure of 1.2 bar and a cathode back pressure of 0 bar. As the current density gradually increases, the local reverse current caused by the pinhole disappears. At 400 mA/cm^2, the voltage drops sharply below 0.5 V. Therefore, during fuel cell operation, if the anode back pressure exceeds the cathode back pressure, the sealing effect of water on pinholes is weakened. When a pressure difference exists between the operating back pressure of the cathode and anode, pinholes are fatal to the fuel cell and may cause a sharp drop in voltage or even burns.

3.8. Effects of small-sized pinholes on temperature distribution under an anode overpressure 1.2 bar at different current densities

Temperature distributions under the above operating conditions are shown in Fig. 12.

Comparing the results shown in Tables 2 and 3 suggests that the temperature changes caused by differently sized pinholes are distinct. For a relatively small pinhole, the hydrogen crossover will be relatively small; as such, the exothermic reaction caused by the cathode catalytic layer will be correspondingly weakened. Meanwhile, according to De Moor et al. [19], when the PEMFC is in an advanced state of degradation, the catalytic layer cannot effectively assure the heat release of hydrogen and oxygen to generate local hot spots owing to the loss of Pt, carbon support, and binder combustion. Because our experiment directly drills into the CCM, the size of the holes is positively correlated with the local hot spots.

4. Conclusions

Herein, pinholes of different sizes were fabricated on CCMs with an area of 50 cm^2 and characterized using PCB technology to investigate the effects of pinholes on PEMFC current density and temperature distributions. The main conclusions are as follows:

(1) Unlike PEMFC operation at high temperature, the PEMFC studied herein generates more water with increasing current density. Owing to the swelling effect of the membrane and the relatively small diffusion coefficient of hydrogen in water, the effects of pinholes on local current density decrease with increasing overall current density.

(2) A certain pressure must be applied to remove water in the pinhole such that hydrogen can reach the cathode directly to perform the HOR reaction. Under this condition, the current is a local reverse current and hydrogen diffuses along with the direction of gas flow in the cathode, affording hydrogen concentration gradient change.
(3) As the HOR reaction rate is higher than the ORR reaction rate at the cathode, ORR plays a dominant role as hydrogen is consumed under anode overpressure conditions. Further, the output of the overall current density must be satisfied such that the local current density below the cell is higher than the output current density. The highest temperature occurs at the pinhole position, and temperature exhibits the same distribution as cathodic current density.
(4) The local current density characteristics of the pinhole are dependent on pinhole size. Smaller pinholes require greater anode overpressure to generate local reverse current density during PEMFC operation.
(5) The presence of pinholes does not directly affect the performance of PEMFC, especially when the pinholes are relatively small. Owing to the sealing effect, pinholes do not generate local reverse currents and normal operation prevails. However, fuel starvation can occur at the hydrogen outlet, affording an overall decrease in the performance of the cell.

CRediT authorship contribution statement

Feng Ding: Conceptualization, Investigation, Writing – original draft. **Tingting Zou:** Validation. **Tao Wei:** Validation. **Lei Chen:** Writing – review & editing. **Xiaoping Qin:** Writing – review & editing. **Zhigang Shao:** Conceptualization, Supervision, Funding acquisition, Project administration. **Jianjun Yang:** Supervision.

Declaration of Competing Interest

The authors declare that they have no known competing financial interests or personal relationships that could have appeared to influence the work reported in this paper.

Data availability

Data will be made available on request.

Acknowledgments

Funding: This work was financially supported by the National Key Research and Development Program of China (No. 2020YFB0106602).

References

[1] Wang Y, Chen KS, Mishler J, Cho SC, Adroher XC. A review of polymer electrolyte membrane fuel cells: technology, applications, and needs on fundamental research. Appl Energ 2011;88:981–1007. https://doi.org/10.1016/j.apenergy.2010.09.030.
[2] Pei PC, Chen HC. Main factors affecting the lifetime of Proton Exchange Membrane fuel cells in vehicle applications: a review. Appl Energ 2014;125:60–75. https://doi.org/10.1016/j.apenergy.2014.03.048.
[3] Rodgers MP, Bonville LJ, Kunz HR, Slattery DK, Fenton JM. Fuel cell perfluorinated sulfonic acid membrane degradation correlating accelerated stress testing and lifetime. Chem Rev 2012;112:6075–103. https://doi.org/10.1021/cr200424d.
[4] Choi SR, Kim DY, An WY, Choi S, Park K, Yim S-D, et al. Assessing the degradation pattern and mechanism of membranes in polymer electrolyte membrane fuel cells using open-circuit voltage hold and humidity cycle test protocols. Mater Sci Energy Technol 2022;5:66–73. https://doi.org/10.1016/j.mset.2021.12.001.
[5] Collier A, Wang HJ, Yuan XZ, Zhang JJ, Wilkinson DP. Degradation of polymer electrolyte membranes. Int J Hydrogen Energ 2006;31:1838–54. https://doi.org/10.1016/j.ijhydene.2006.05.006.
[6] Ren P, Pei PC, Li YH, Wu ZY, Chen DF, Huang SW. Degradation mechanisms of proton exchange membrane fuel cell under typical automotive operating conditions. Prog Energ Combust 2020;80:100859. https://doi.org/10.1016/j.pecs.2020.100859.
[7] Niroumand AM, Homayouni H, Goransson G, Olfert M, Eikerling M. In-situ diagnostic tools for hydrogen transfer leak characterization in PEM fuel cell stacks part III: Manufacturing applications. J Power Sources 2020;448:227359. https://doi.org/10.1016/j.jpowsour.2019.227359.
[8] Moor GD, Charvin N, Bas C, Caqué N, Rossinot E, Flandin L. In situ quantification of electronic short circuits in PEM fuel cell stacks. IEEE Trans Ind Electron 2015;62:5275–82. https://doi.org/10.1109/TIE.2015.2395390.
[9] Yuan X-Z, Zhang S, Ban S, Huang C, Wang H, Singara V, et al. Degradation of a PEM fuel cell stack with Nafion® membranes of different thicknesses. Part II: ex situ diagnosis. J Power Sources 2012;205:324–34. https://doi.org/10.1016/j.jpowsour.2012.01.074.
[10] Kreitmeier S, Schuler GA, Wokaun A, Büchi FN. Investigation of membrane degradation in polymer electrolyte fuel cells using local gas permeation analysis. J Power Sources 2012;212:139–47. https://doi.org/10.1016/j.jpowsour.2012.03.071.
[11] Huang BT, Chatillon Y, Bonnet C, Lapicque F, Leclerc S, Hinaje M, et al. Experimental investigation of pinhole effect on MEA/cell aging in PEMFC. Int J Hydrogen Energ 2013;38:543–50. https://doi.org/10.1016/j.ijhydene.2012.09.058.
[12] Singh Y, Orfino FP, Dutta M, Kjeang E. 3D failure analysis of pure mechanical and pure chemical degradation in fuel cell membranes. J Electrochem Soc 2017;164:F1331–41. https://doi.org/10.1149/2.0451713jes.
[13] Phillips A, Ulsh M, Neyerlin KC, Porter J, Bender G. Impacts of electrode coating irregularities on polymer electrolyte membrane fuel cell lifetime using quasi in-situ infrared thermography and accelerated stress testing. Int J Hydrogen Energ 2018;43:6390–9. https://doi.org/10.1016/j.ijhydene.2018.02.050.
[14] Kundu S, Fowler MW, Simon LC, Grot S. Morphological features (defects) in fuel cell membrane electrode assemblies. J Power Sources 2006;157:650–6. https://doi.org/10.1016/j.jpowsour.2005.12.027.
[15] Cho Y-H, Park H-S, Kim J, Cho Y-H, Won Cha S, Sung Y-E. The operation characteristics of MEAs with pinholes for polymer electrolyte membrane fuel cells. Electrochem Solid St 2008;11:B153. https://doi.org/10.1149/1.2937450.
[16] Ramani D, Singh Y, White RT, Haddow T, Wegener M, Orfino FP, et al. Four-dimensional in situ imaging of chemical membrane degradation in fuel cells. Electrochim Acta 2021;380:138194. https://doi.org/10.1016/j.electacta.2021.138194.
[17] Robert M, El Kaddouri A, Crouillere M, Perrin J-C, Dubau L, Dubelley F, et al. A chemical-mechanical ex-situ aging of perfluorosulfonic-acid membranes for fuel cells: impact on the structure and the functional properties. J Power Sources 2022;520:230911. https://doi.org/10.1016/j.jpowsour.2021.230911.
[18] Obermaier M, Jozwiak K, Rauber M, Bauer A, Scheu C. Comparative study of pinhole detection methods for automotive fuel cell degradation analysis. J Power Sources 2021;488:229405. https://doi.org/10.1016/j.jpowsour.2020.229405.
[19] De Moor G, Bas C, Charvin N, Dillet J, Maranzana G, Lottin O, et al. Perfluorosulfonic acid membrane degradation in the hydrogen inlet region: a macroscopic approach. Int J Hydrogen Energ 2016;41:483–96. https://doi.org/10.1016/j.ijhydene.2015.10.066.
[20] Inaba M, Kinumoto T, Kiriake M, Umebayashi R, Tasaka A, Ogumi Z. Gas crossover and membrane degradation in polymer electrolyte fuel cells. Electrochim Acta 2006;51:5746–53. https://doi.org/10.1016/j.electacta.2006.03.008.
[21] Jung A, Oh J, Han K, Kim MS. An experimental study on the hydrogen crossover in polymer electrolyte membrane fuel cells for various current densities. Appl Energ 2016;175:212–7. https://doi.org/10.1016/j.apenergy.2016.05.016.
[22] Vilekar SA, Datta R. The effect of hydrogen crossover on open-circuit voltage in polymer electrolyte membrane fuel cells. J Power Sources 2010;195:2241–7. https://doi.org/10.1016/j.jpowsour.2009.10.023.
[23] Weber AZ. Gas-crossover and membrane-pinhole effects in polymer-electrolyte fuel cells. J Electrochem Soc 2008;155:B521–31. https://doi.org/10.1149/1.2898130.
[24] Kusoglu A, Weber AZ. A mechanistic model for pinhole growth in fuel-cell membranes during cyclic loads. J Electrochem Soc 2014;161:E3311–22. https://doi.org/10.1149/2.036408jes.
[25] Chakraborty U. Fuel crossover and internal current in proton exchange membrane fuel cell modeling. Appl Energ 2016;163:60–2. https://doi.org/10.1016/j.apenergy.2015.11.012.
[26] Zheng W, Xu L, Hu Z, Ding Y, Li J, Ouyang M. Dynamic modeling of chemical membrane degradation in polymer electrolyte fuel cells: effect of pinhole formation. J Power Sources 2021;487:229367. https://doi.org/10.1016/j.jpowsour.2020.229367.
[27] Singh R, Sui PC, Wong KH, Kjeang E, Knights S, Djilali N. Modeling the effect of chemical membrane degradation on PEMFC performance. J Electrochem Soc 2018;165:F3328–36. https://doi.org/10.1149/2.0351806jes.
[28] Nguyen TT, Fushinobu K. Effect of operating conditions and geometric structure on the gas crossover in PEM fuel cell. Sustain Energy Techn 2020;37:100584. https://doi.org/10.1016/j.seta.2019.100584.
[29] Lin R, Gulzow E, Schulze M, Friedrich KA. Investigation of membrane pinhole effects in polymer electrolyte fuel cells by locally resolved current density. J Electrochem Soc 2011;158:B11–7. https://doi.org/10.1149/1.3504255.
[30] Reshetenko TV, Bender G, Bethune K, Rocheleau R. Application of a segmented cell setup to detect pinhole and catalyst loading defects in proton exchange membrane fuel cells. Electrochim Acta 2012;76:16–25. https://doi.org/10.1016/j.electacta.2012.04.138.
[31] Garcia-Sanchez D, Morawietz T, da Rocha PG, Hiesgen R, Gazdzicki P, Friedrich A. Local impact of load cycling on degradation in polymer electrolyte fuel cells. Appl Energ 2020;259:114210. https://doi.org/10.1016/j.apenergy.2019.114210.
[32] Yin C, Cao JS, Tang QL, Su YH, Wang RK, Li K, et al. Study of internal performance of commercial-size fuel cell stack with 3D multi-physical model and high resolution

current mapping. Appl Energ 2022;323:119567. https://doi.org/10.1016/j.apenergy.2022.119567.
[33] Shan J, Gazdzicki P, Lin R, Schulze M, Friedrich KA. Local resolved investigation of hydrogen crossover in polymer electrolyte fuel cell. Energy 2017;128:357–65. https://doi.org/10.1016/j.energy.2017.03.104.
[34] Liu DC, Lin R, Feng BW, Han LH, Zhang Y, Ni M, et al. Localised electrochemical impedance spectroscopy investigation of polymer electrolyte membrane fuel cells using Print circuit board based interference-free system. Appl Energ 2019;254:113712. https://doi.org/10.1016/j.apenergy.2019.113712.
[35] Miao TW, Tongsh CS, Wang JN, Cheng P, Liang JQ, Wang ZX, et al. Current density and temperature distribution measurement and homogeneity analysis for a large-area proton exchange membrane fuel cell. Energy 2022;239:121922. https://doi.org/10.1016/j.energy.2021.121922.
[36] Peng LF, Shao H, Qiu DK, Yi PY, Lai XM. Investigation of the non-uniform distribution of current density in commercial-size proton exchange membrane fuel cells. J Power Sources 2020;453:227836. https://doi.org/10.1016/j.jpowsour.2020.227836.
[37] Eikerling MH, Berg P. Poroelectroelastic theory of water sorption and swelling in polymer electrolyte membranes. Soft Matter 2011;7:5976. https://doi.org/10.1039/c1sm05273j.
[38] Kreitmeier S, Michiardi M, Wokaun A, Buchi FN. Factors determining the gas crossover through pinholes in polymer electrolyte fuel cell membranes. Electrochim Acta 2012;80:240–7. https://doi.org/10.1016/j.electacta.2012.07.013.
[39] Lu WZ, Liu ZX, Wang C, Mao ZQ, Zhang ML. The effects of pinholes on proton exchange membrane fuel cell performance. Int J Energ Res 2011;35:24–30. https://doi.org/10.1002/er.1728.
[40] Weber AZ, Newman J. Transport in polymer-electrolyte membranes – II. Mathematical model. J Electrochem Soc 2004;151:A311–25. https://doi.org/10.1149/1.1639157.
[41] Haase S, Moser M, Hirschfeld JA, Jozwiak K. Current density and catalyst-coated membrane resistance distribution of hydro-formed metallic bipolar plate fuel cell short stack with 250 cm(2) active area. J Power Sources 2016;301:251–60. https://doi.org/10.1016/j.jpowsour.2015.09.118.